PRELIMINARY EVALUATION OF THE AIRBORNE IMAGING SPECTROMETER FOR VEGETATION ANALYSIS IN THE KLAMATH NATIONAL FOREST OF NORTHEASTERN CALIFORNIA

Alan H. Strahler

Curtis E. Woodcock

Francisco X. Avila

Department of Geology and Geography

Hunter College

City University of New York

Final Report

JPL Contract No. 956585

May 31, 1985

HC/CUNY DGG

Technical Report 85-1

This report was prepared for the Jet Propulsion Laboratory, California Institute of Technology, sponsored by the National Aeronautics and Space Administration.

TABLE OF CONTENTS

1. INTRODUCTION

The purpose of this report is to document the experiences and results associated with a project entitled "Preliminary Evaluation of the Airborne Imaging Spectrometer for Vegetation Analysis." The primary goal of the project was to provide ground truth, manual interpretation, and computer processing of data from an experimental flight of the Airborne Infrared Spectrometer (AIS) to determine the extent to which high spectral resolution remote sensing could differentiate among plant species, and especially species of conifers, for a naturally vegetated test site. Through the course of the research, JPL acquired AIS imagery of our test areas in the Klamath National Forest, northeastern California, on two overflights: one in June, 1983, of the Dock Well transect, and a second in August, 1983, of both the Dock Well and Grass Lake transects. Over the next year or so, we also received three generations of data: first overflight, second overflight, and reprocessed second overflight. Two field visits were made: one trip immediately following the first overflight to note snow conditions and temporally-related vegetation states at the time of the sensor overpass; and a second trip about six weeks later, following acquisition of prints of the images from the first AIS overpass.

2. BACKGROUND

The scientific basis of remote sensing of earth resources is that different substances reflect (or emit)

radiation with different intensities in different regions of the electromagnetic spectrum (EMS). To date, remote sensing from spacecraft has been dominated by the analysis of radiance data integrated over broad bands of the EMS. The most common data available are from the Landsat Multispectral Scanner (MSS), which has three (nominal) spectral bands 100nm wide, and one spectral band 300nm wide, in the visible and near-infrared portions of the spectrum. Due to the small number of bands and their coarse spectral resolution, much work in remote sensing has centered on statistical information extraction techniques, rather than an improved understanding of reflectance spectra and their resulting radiance spectra.

A newer sensor, the Thematic Mapper (TM), presents an improvement, providing six bands of data from the visible to the shortwave infrared (the thermal band is not considered here). However, these bands are still relatively broad, ranging from 70nm at 0.45 um to 270nm at 2.08 um. While this sensor is an improvement over the MSS, its band width severly limits the analysis of reflectance spectra. Preliminary indications are that the analysis of TM data will continue along the lines of statistically-based empirical procedures similar to those used with MSS data.

The AIS measures reflected radiance over the near-infrared portion of the EMS from 1.2 to 2.4 um [1]. For the overflight of our Goosenest study area, in the Goosenest

Ranger District of the Klamath National Forest, the AIS was configured to collect 32 bands 9.6 nm wide in one of four wavelength regions: nominally 1.2-1.5 um, 1.5-1.8 um, 1.8-2.1 um, and 2.1-2.4 um. For each of two test sites, three overpasses were made, omitting data collection in the 2.1-2.4 um band. In addition to the AIS, 35mm black and white photography of each flight line was taken to help locate the narrow AIS strip.

3. PHASE I

3.1. FIRST FIELD VISIT

The first field visit occurred immediately following the first overpasses of the AIS. Its primary objective was to note the phenological state of the various plant species, and also note the extent of snow cover. Snow cover was expected to be unimportant at the time the original proposal was submitted, but due to record snowfall in 1983 it was necessary to know which features in the imagery would be attributable to snow.

Due to the narrow swath width of the AIS (900m), it was important to determine the flight path for each overpass of the study area. At NASA-Ames immediately following the return of the C-130, the video tapes from a bore-sighted TV camera taken during each of the overpasses were studied and a line approximating the center of each overpass was sketched on 1:24000 color air photos for use in the field. These lines were helpful in limiting the area requiring

ground truth, but lacked accuracy because oil accidentally covered the lens of the video camera during the flight. (The data from the AIS and the 35mm camera were not available for this field visit because of the processing required prior to their use.)

During the field visit, various areas along each flightline were visited, and detailed notes about the vegetation at the sites were made. In addition, 35mm slides using standard color and color-infrared film were taken using two comparable cameras. These slides served two purposes: 1) to document the site at the time of the overpass; and 2) to give a preliminary indication of the reflectance of various plant species and vegetation types in the visible and near-infrared wavelengths. These photographs are only capable of providing an initial indication, because color-infrared film is sensitive to different wavelengths than the AIS.

The first test site, referred to as the "Grass Lake" site, consists of a transect with a northeast-southwest orientation. At the southwest end is Herd Peak and an interesting gradient of tree species. At the highest elevation, red fir is the dominant tree species, giving way down slope to a mixed conifer forest that is often dominated by white fir. Other tree species common in this mixed conifer area are incense cedar, Douglas fir, and ponderosa and Jeffrey pine. Figure 1 presents color and color-infrared

prints of a mixed conifer stand in the Herd Peak area. The tallest tree is a Douglas fir and the two shorter trees to the left are a white fir and a ponderosa pine (far left). The original transparency reveals some subtle differences in spectral tone between the two species that is not readily visible in the prints.

Below Herd Peak in the transect is Grass Lake, which is fairly large (approximately 3 miles long) but very shallow. In fact, at certain times of the year the lake is almost dry. As a result, there are interesting patterns of different species of grasses that grow throughout the lake and along its shore, providing considerable variety for spectral differentiation. Figure 2 shows a general view of Grass Lake from the southwest, pointing approximately in the direction of the AIS overpass. At the time of the overpass, the Lake was relatively full due to the high precipitation of the preceeding winter. The white areas in the Lake are dead grasses killed by high water levels. The photos in Figure 3 were taken from the Lake's edge and show the variety of grasses common around the Lakes's border. Several distinct zones of grasses are visible descending from the dry shoreline into the shallow waters along its edge.

Northeast of Grass Lake is an area that is relatively flat and has vegetative types similar to high desert habitats. The area is characterized by sparsely stocked pon-

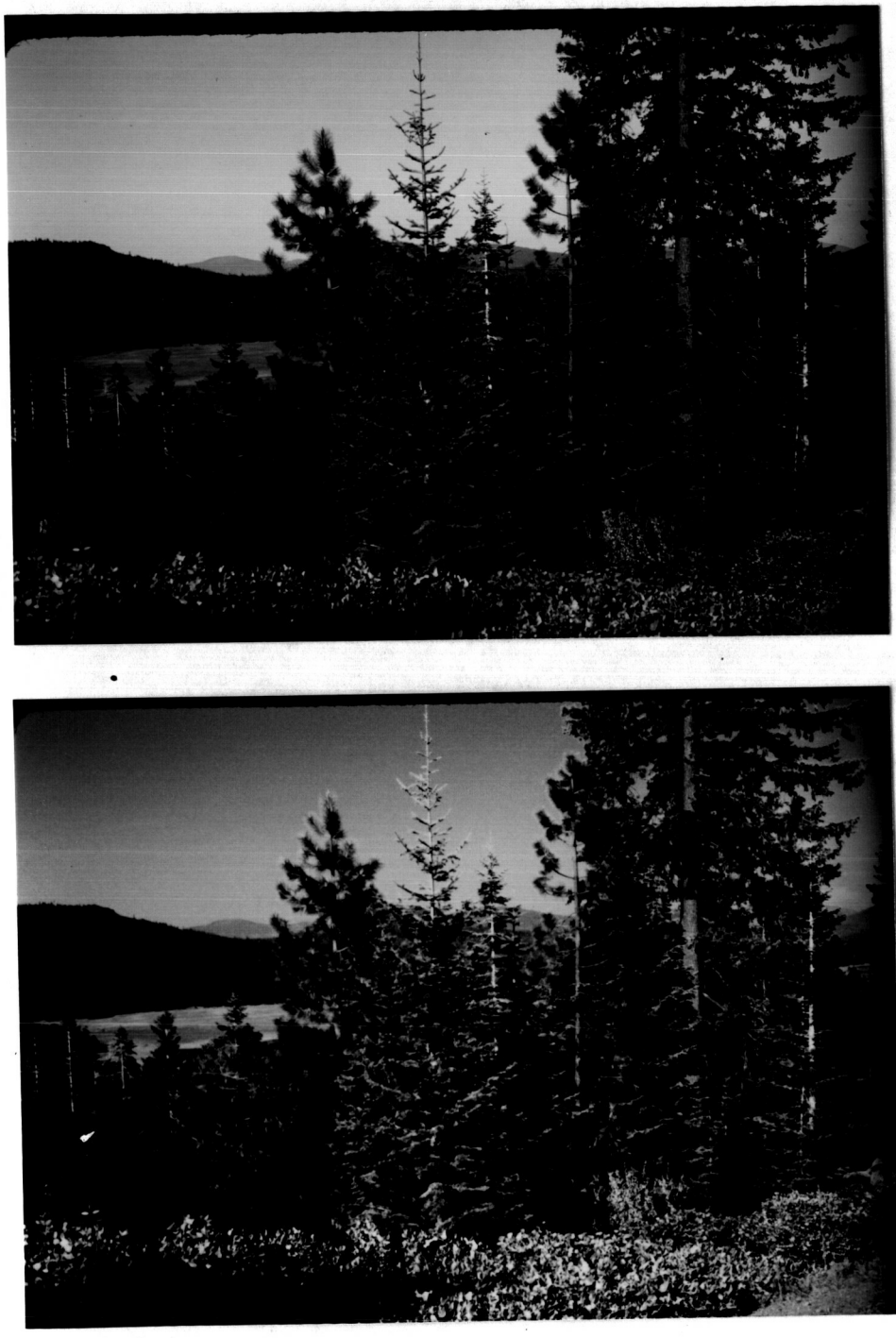

Figure 1. Color and color-infrared pictures of a mixed conifer stand in the Grass Lake test site. The tall tree in back is a Douglas fir, with a white fir and ponderosa pine in the left side of the picture.

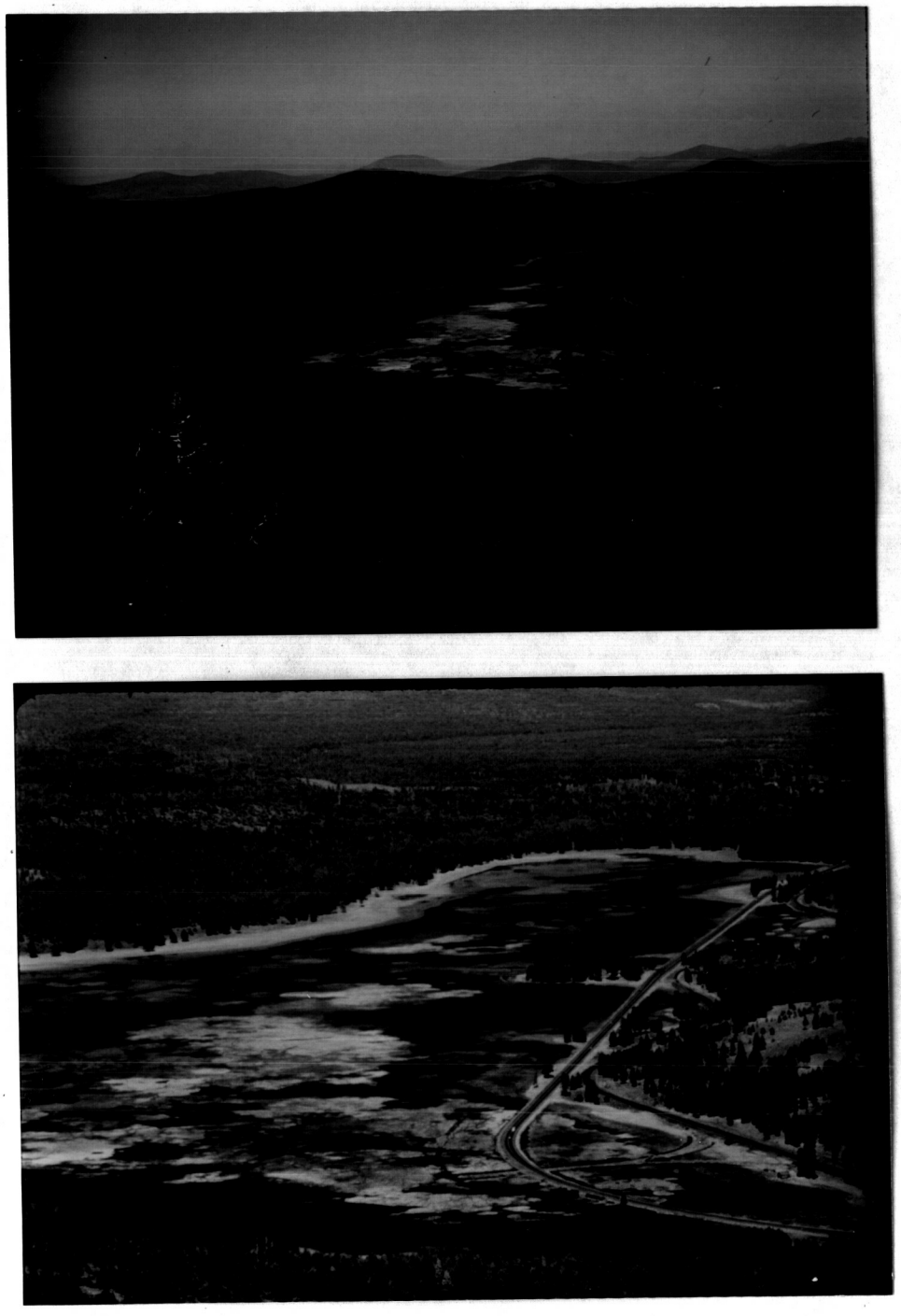

Figure 2. Views of Grass Lake. The variations in depth of the Lake and patterns of dead and healthy grasses in the middle of the lake and along its edges are easily distinguished in the photos.

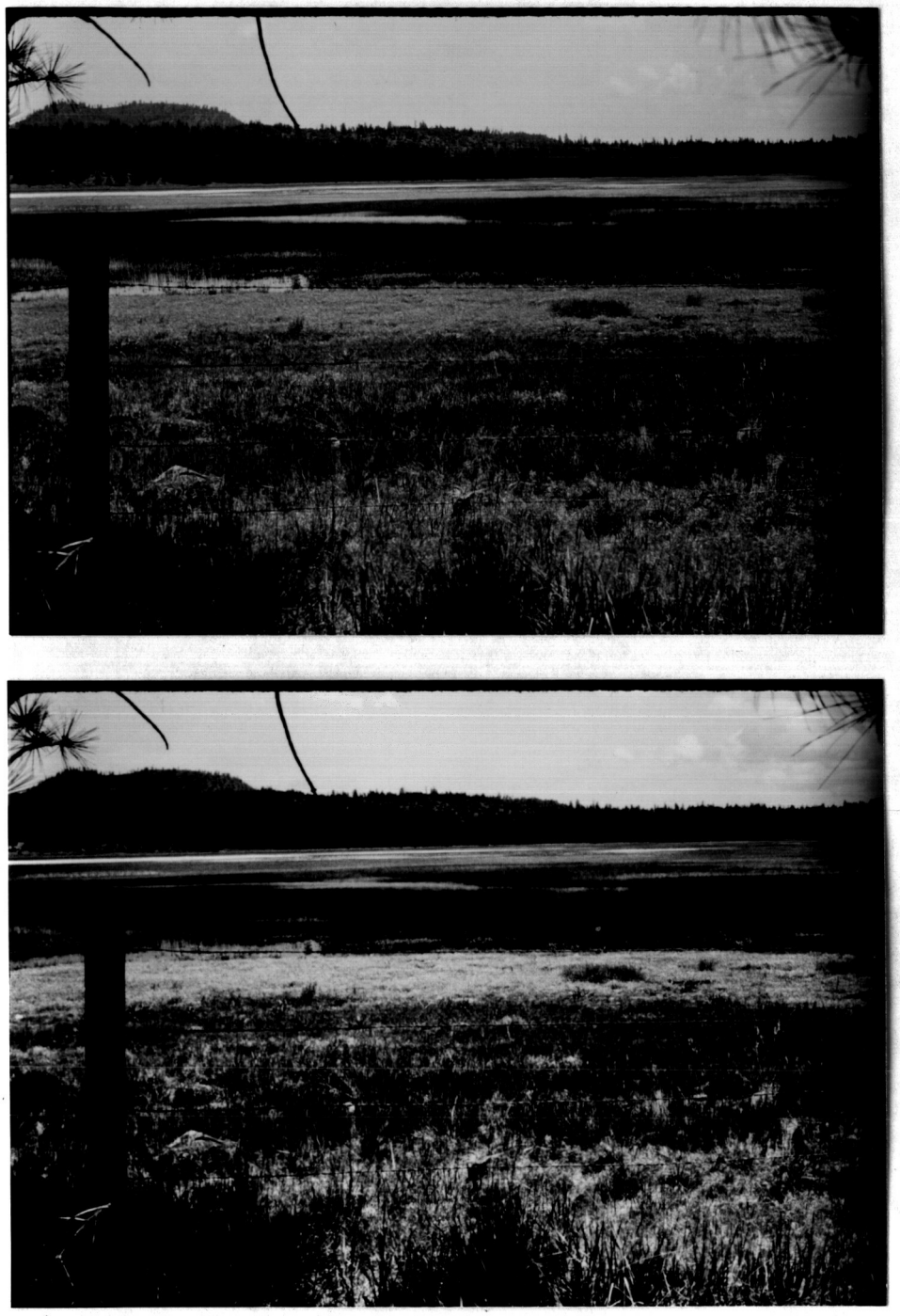

Figure 3. Area at the edge of Grass Lake. Notice the zones of different grasses and their variation in reflectance in both the visible and near-infrared wavelengths.

derosa and Jeffrey pine and an extensive understory of brush comprised of antelope bush (Purshia tridentata) (shown in Figure 4), manzanita (Arctostaphylos spp.), great basin sage (Artemisia tridentata), and rabbit brush (Chrysothamnus spp.). In addition, there are several lava flows in the area that are distinctively marked by dense patches of mountain mahogany (Cercocarpus betuloides) that grow along their margins. Figure 5 shows a typical mix of brush and sparse pines in the northeast portion of the Grass Lake transect.

The second test transect runs in a north-south direction and is considerably east of the Grass Lake test site. We refer to this test site as the "Dock Well" area, and it has two distinctive sections. The northern section is very flat and is similar to the "high desert" area described in the Grass Lake site in that it is sparsely stocked with ponderosa and Jeffrey pines. However, the understory brush in this test site grows considerably lower and tends to be more spatially homogeneous. As a result, this area gives a close approximation to a simple model of individual trees on a homogeneous background. A simple scene such as this has proved useful in past exploratory research where the number of convolving factors are minimized. Figure 6 presents the general appearance of the flat northern section of the Dock Well test site.

The second part of the Dock Well site is a long, gentle hillslope that leads to a ridge at the extreme southern end

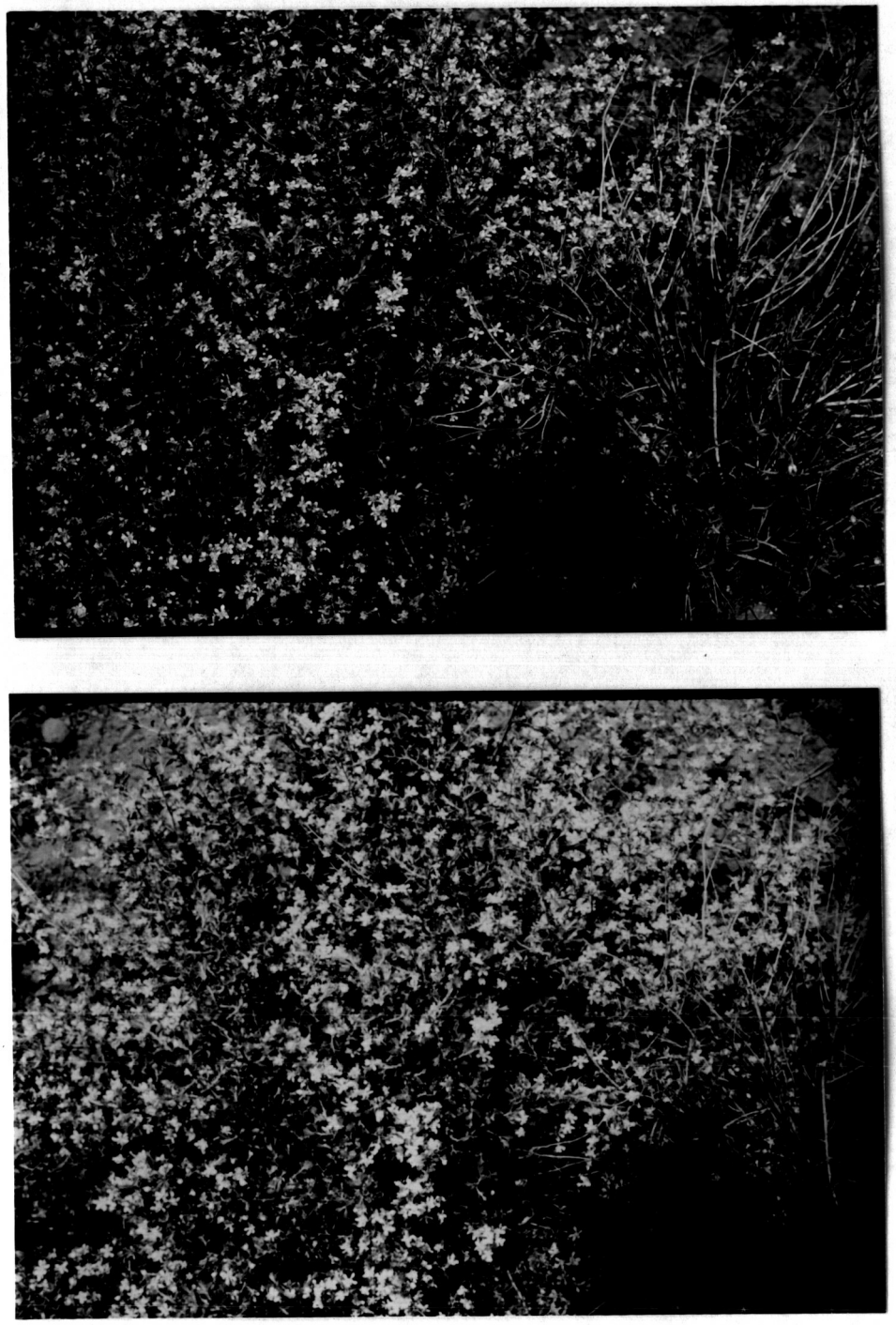

Figure 4. Antelope bush (Purshia tridentata).

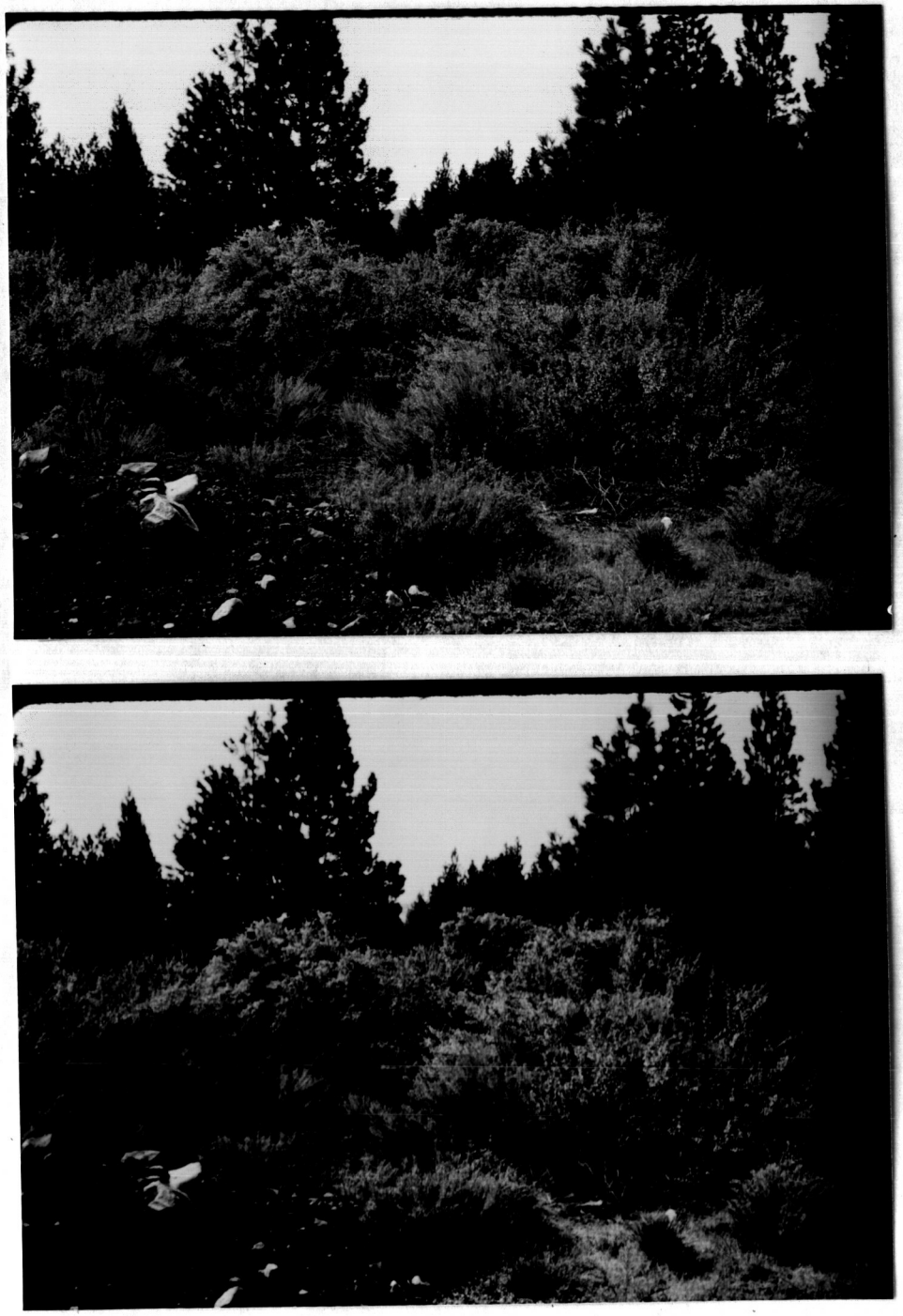

Figure 5. A mix of brush and trees characteristic of the northeast portion of the Grass Lake test site. Note the variation in reflectance among brush species and between the trees and the brush.

Figure 6. View of northern section of the Dock Well test site.

of the transect. There is a gradual change in tree species composition as elevation increases. At the bottom of the slope the area is similar to the high desert area previously described. As elevation increases, the forest canopy becomes more dense, the trees become bigger, and some white fir is present. Eventually white fir becomes dominant, incense cedar is present, and the pines become more scarce. At the highest elevations, red fir becomes the dominant species with white fir still present but less frequent. This gradation of tree species provides an interesting opportunity to explore the spectral reflectance of different conifer species.

Figure 7 shows three tree species in the mixed conifer area of the test site. The tall trees in the back are ponderosa pine, the tree in the front left is incense cedar, and the tree in the front right is white fir. Subtle differences in the tone in both the color and infrared prints can be seen for the different tree species, suggesting the possibility different reflectance spectra for these species throughout both the visible and near-infrared portion of the EMS.

3.2. SECOND FIELD VISIT

Prior to the second field visit, we received the roll of negatives from the 35mm camera and had 8x10 prints made of each frame. The AIS data were not received until we were in the field. The data only included the Dock Well site and

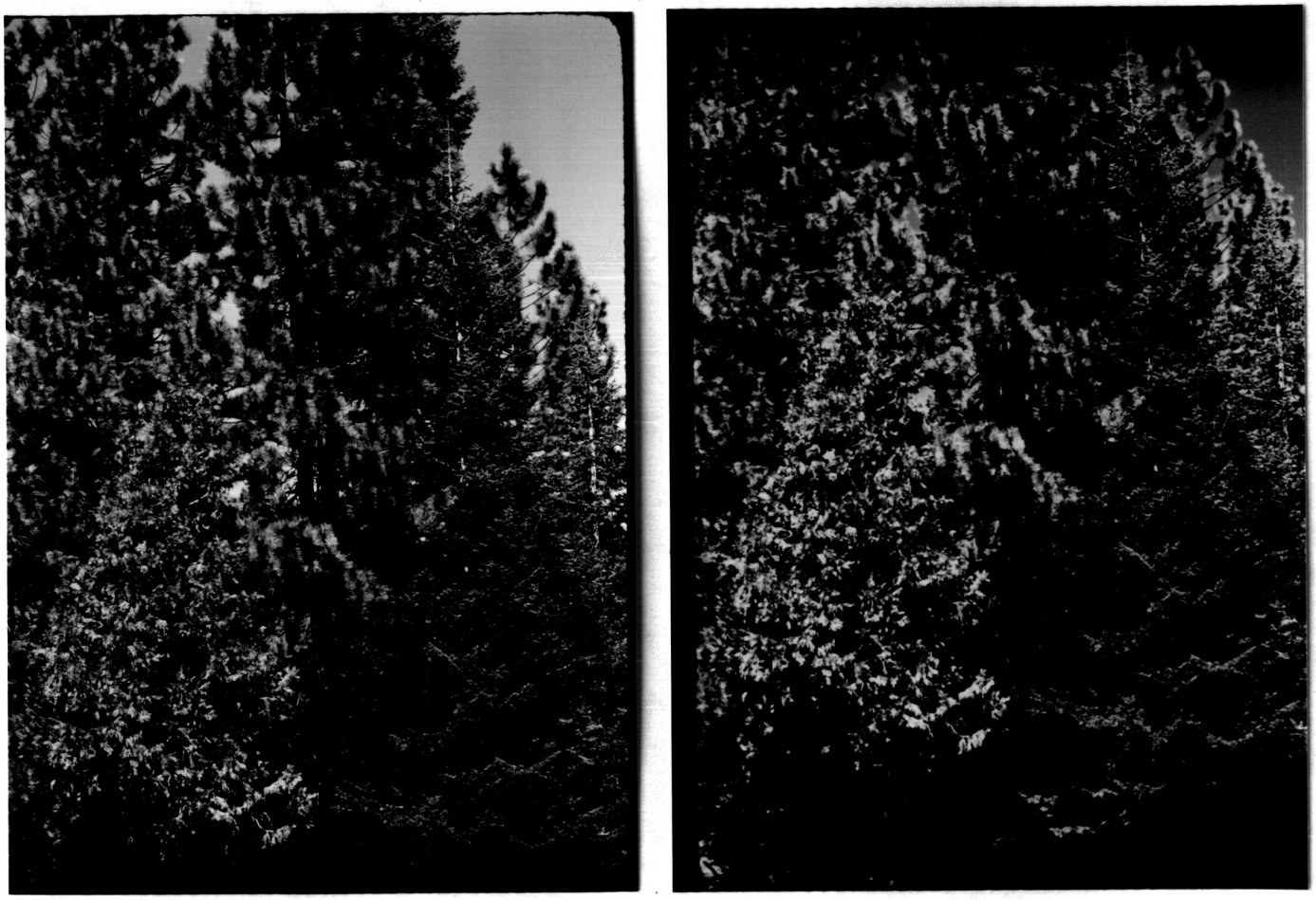

Figure 7. Three tree species in the mixed conifer area of the Dock Well test site. The two large trees in the back are ponderosa pines; a small incense cedar is in the lower left, and a small white fir is in the lower right.

consisted of three large prints for each of the three passes over the site (one for each grating position). It was unfortunate that the data from the Grass Lake site were unavailable, as this site had the most obvious features and would have been the easier of the two sites on which to begin work. Also, there was no snow on the Grass Lake transect at the time of the overpass.

Considerable time was required to determine how the prints for each grating position fit together. The poor quality of the data made it difficult to identify objects present in both images. In addition, the separate processing of each print made the areas of overlap on adjoining prints very difficult to recognize. This problem is readily apparent when the overlapping areas of Figures 8A, 8B and 8C are compared. Another problem related to the separate processing of different parts of a single flightline is the dark banding found in some parts of the data. Since this banding does not occur uniformly throughout single flightlines and is confined to individual prints, it is assumed to be an artifact of the image processing.

There are a couple of additional suggestions we would like to make regarding the processing of the data. First, the use of Gaussian stretches may not be advisable because they tend to concentrate a large number of the pixels in the middle grey tones, limiting the contrast in the image. The images might be more easily interpreted following an equal

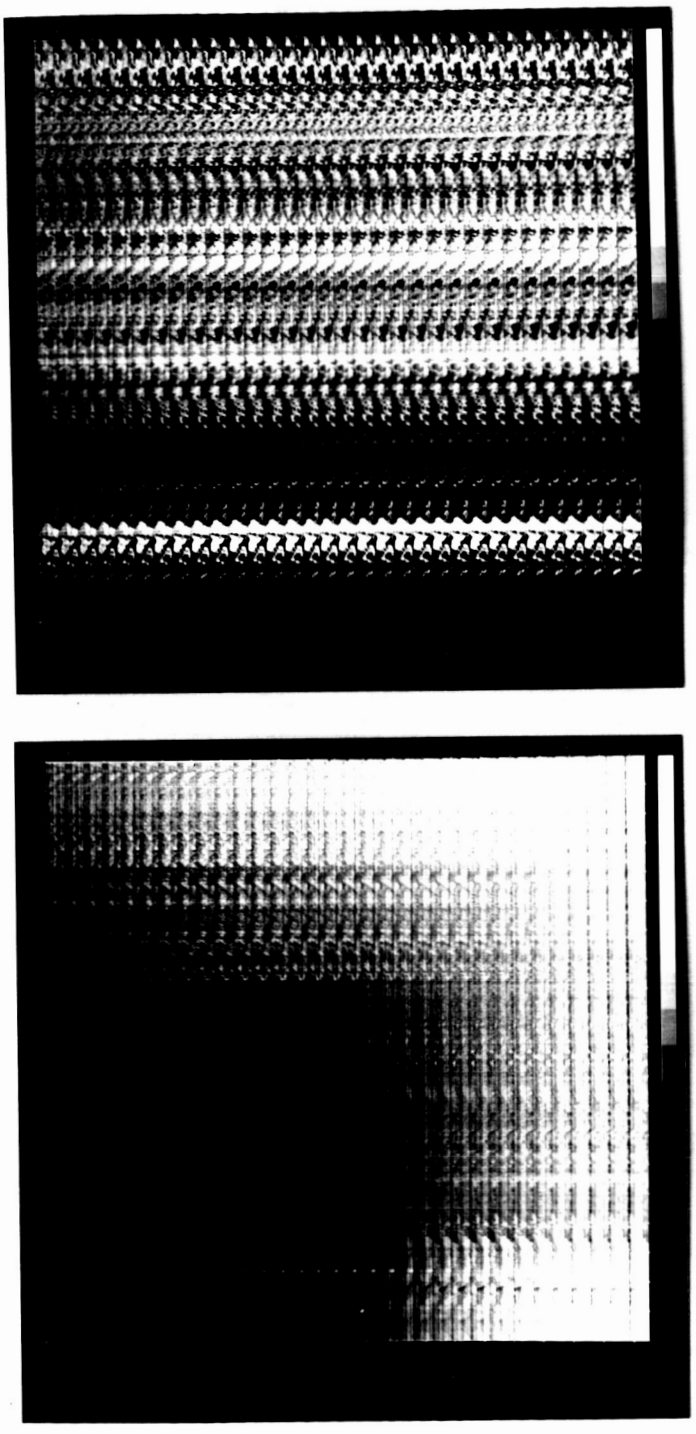

ORIGINAL PAGE IS
OF POOR QUALITY

Figures 8A and 8B. Upper photo (A): north end of GPOS 1 overflight. Lower photo (B): center section of overflight.

area stretch or another similar technique. A second suggestion concerns spectral filtering. Spectral filtering for the replacement of missing values makes sense for this imagery, but any broad spectral filtering based on a running means algorithm (averaging with equal weights for all pixels used) rather than methods that weight the contribution to the output value as a function of their distance can produce artifacts in the resulting spectra [2].

While the quality of the prints was poor, and the features they exhibited were sometimes puzzling and confusing, we were nonetheless able to locate two areas on the ground that showed interesting characteristics on the AIS GPOS 1 imagery. The first of these was a cinder cone, which is visible on the AIS print as a group of three related crescent shapes at the 1.5 um end of the image, and as a rounded form at the 1.8 um end (Figure 9). Field reconnaissance of the cone revealed three types of ejecta present at the surface: red, black, and white (Figure 10). Representative samples of each type of rock were collected and sent to JPL in the fall of 1983.

An examination of accompanying Nikon camera photographs of the cinder cone shows that most of the cone was covered by snow at the time of the overpass. The crescentic shapes at the 1.5 um end of the AIS image are simply areas of ejecta that are not snow covered. Since snow absorbs in the shorter wavelengths in this region, it appears dark on the

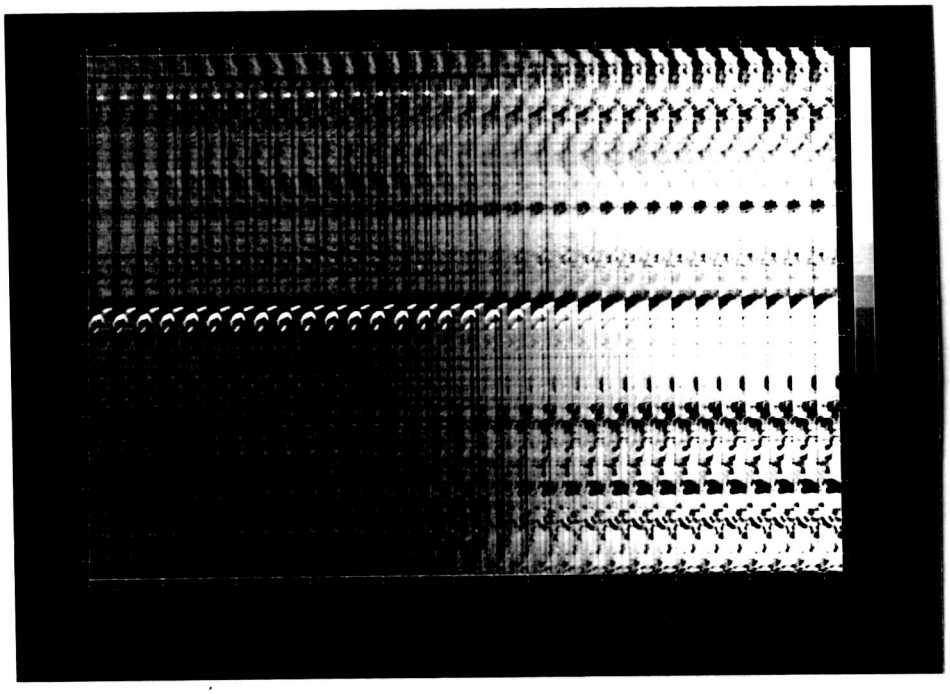

Figure 8C. South end of GPOS 1 overflight.

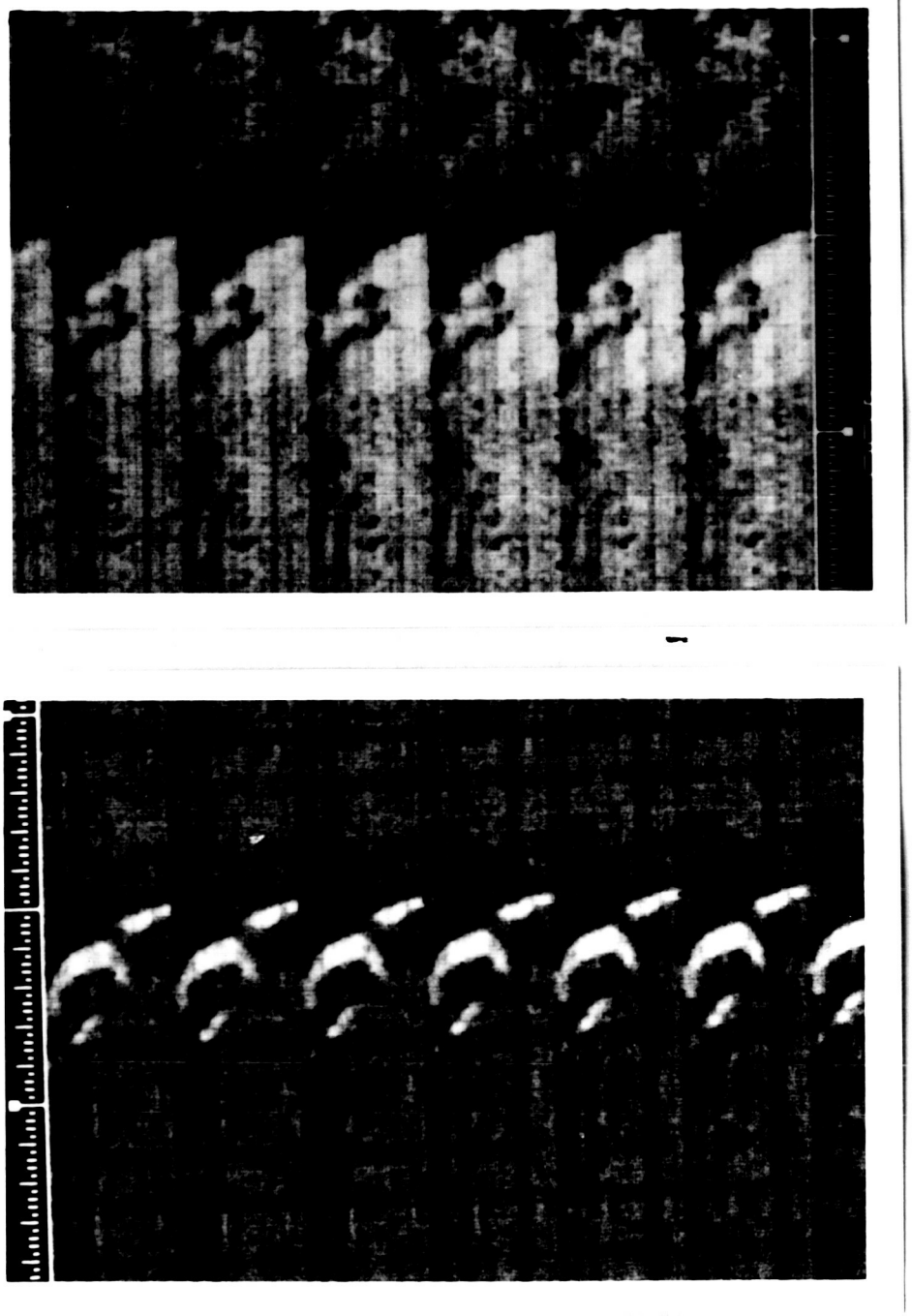

Figure 9. Blowups of the 1.5 um (upper picture) and 1.8 um (lower picture) ends of the AIS flightline for GPOS 1 showing a cinder cone.

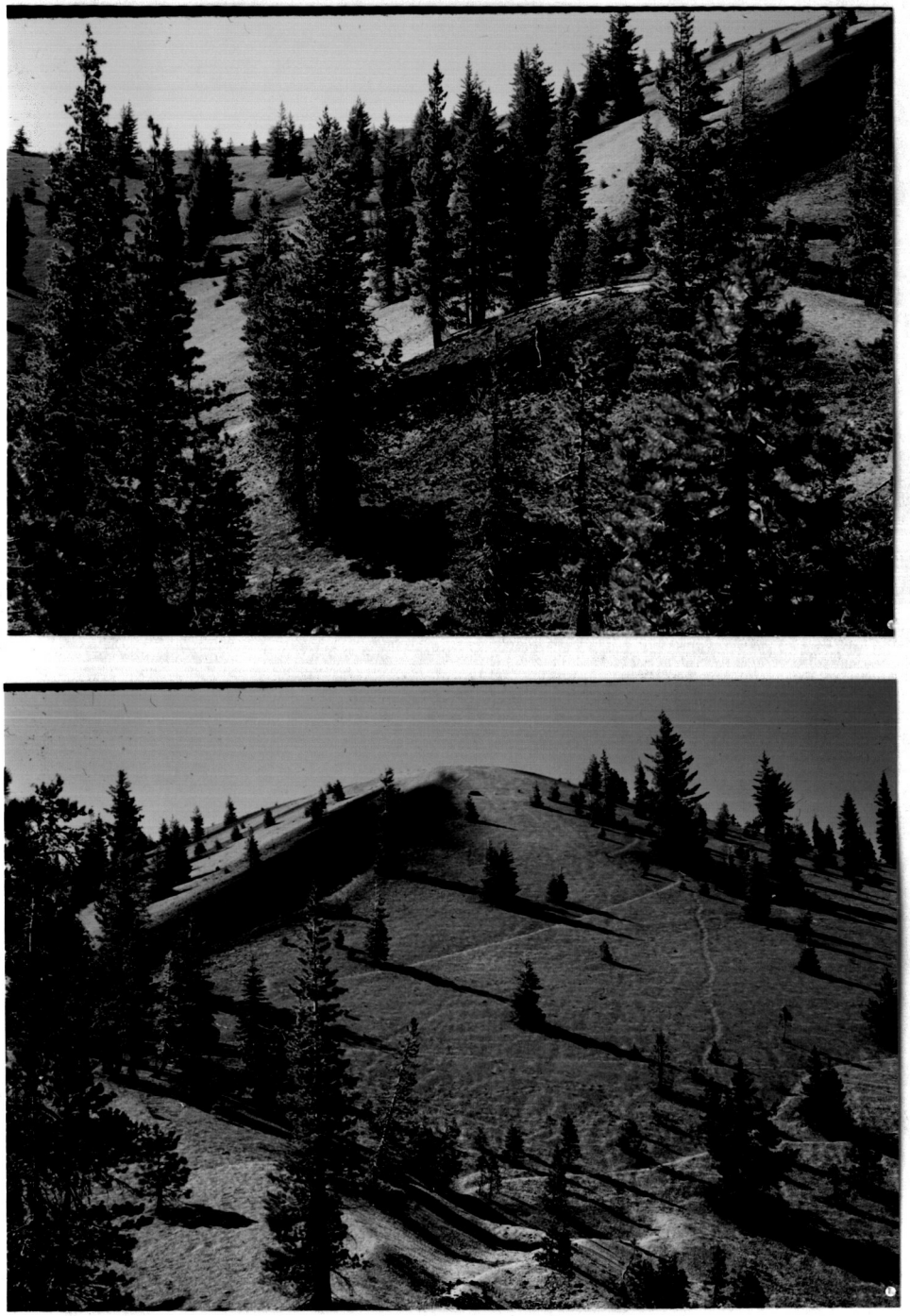

Figure 10. General appearance of the cinder cone shown on AIS imagery in Figure 9.

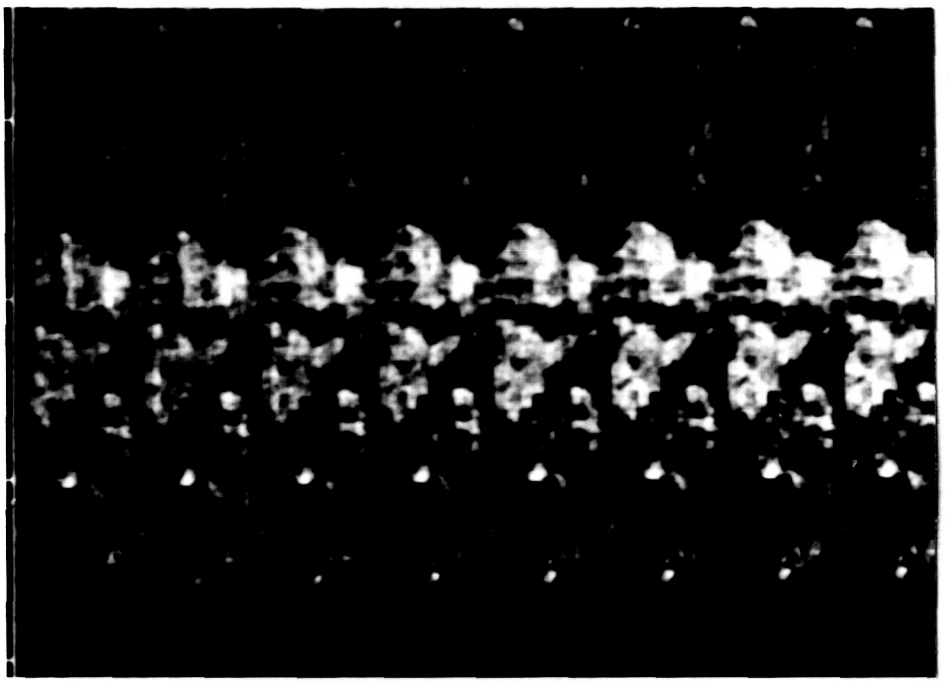

Figure 11. Blowup of the portion of the GPOS 1 print of the area of scarified soil.

AIS image. At the longer wavelengths of the AIS image, the conical shape is much better revealed. Further, there appear to be subtle differences in shading between light and medium grey tones that correspond roughly to the distribution of red and black ejecta, as compared to the lighter-colored pyroclastic materials. Since these materials were obscured by snow, this relation may be artifactual, or coincidentally related to the topography. We are unaware of whether or not there is significant penetration of snow by light at these wavelengths to allow actual sensing of the surface.

Another interesting area taken from the 1.5-1.8 um image that we were able to identify on the ground is shown in Figure 11. As the accompanying panchromatic photo (Figure 12) shows, the feature is not spectrally distinguishable in the visible. However, it presents a high reflectance (bright aspect) in the shortwave infrared. Ground reconnaissance (Figure 13) revealed this area as a very recent clearcut, in which the ground surface had been disturbed and the logging slash had been piled up for burning using heavy equipment. Although the preprocessing of the AIS imagery leaves us somewhat uncertain as to whether or not light tones indicate high reflectance, the scarified soil suface is quite distinctive.

3.3. SECOND OVERPASS

Following improvements of the AIS, a second overpass of both the Grass Lake and Dock Well test sites was flown. On January 12th, we visited JPL and received tapes containing the imagery for both sites, and contact prints of the Nikon 35mm photography. In addition, we were briefed on recent developments in image processing software designed for analysis of data from the AIS.

During our visit, we also spent some time looking at the imagery from the new flight on the interactive display monitor. It was readily apparent that the quality of the data from the new flight was far superior to the original data we had examined. While we were looking at the AIS

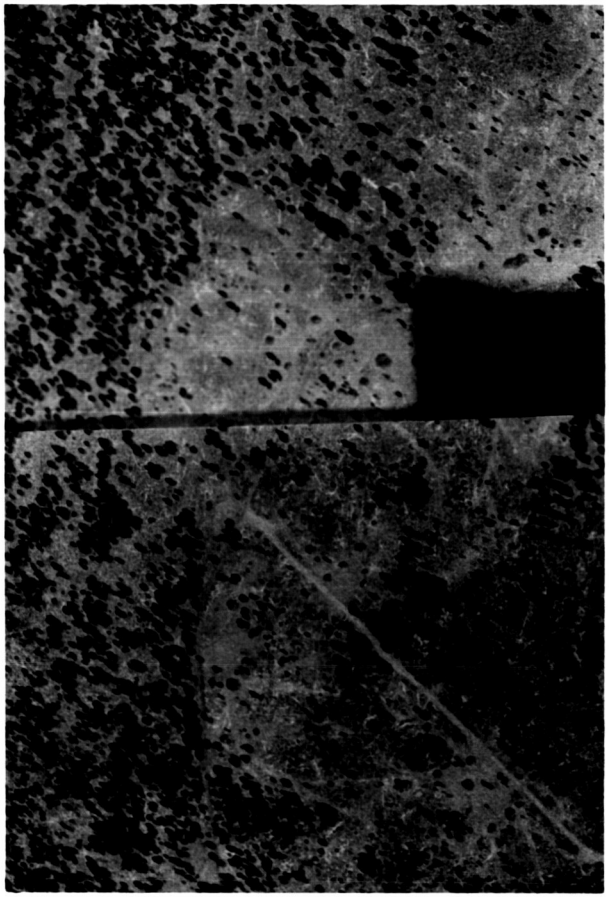

Figure 12. Portion of two Nikon camera prints taken during the AIS overpass. This picture corresponds to the area in the AIS print shown in Figure 11.

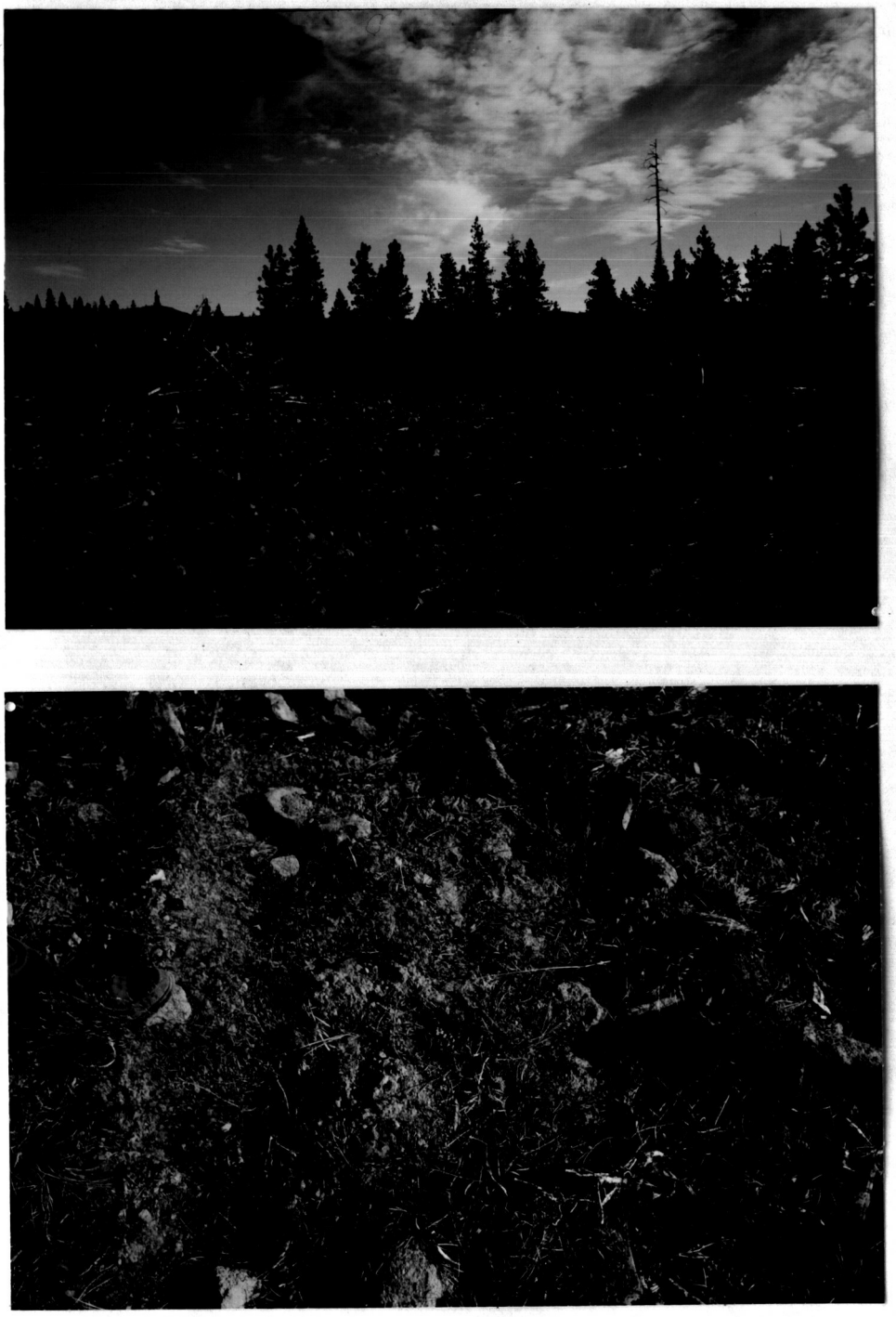

Figure 13. Scarified soil surface identified on AIS imagery (Figure 11). The upper picture presents a general view of the area, and the lower picture shows a close-up of the soil surface.

imagery, we used the new JPL software to plot spectra of several forest species for Grating Position 0 (1.5-1.8 um) and 1 (1.8-2.1 um). While these graphs should not be interpreted as true "reflectance spectra" because there is no correction for variation in available radiance at different wavelengths or for atmospheric effects, they show some interesting features.

The most obvious feature in the graph for Grating Position 0 (Figure 14) is the variation in the overall magnitude of reflectance for the four areas analyzed. In addition, the shapes of the graphs for each area show some subtle, but possibly important differences. Two peaks in reflectance for each area can be seen; the first one near 1.59 um and the second near 1.65 um. Interestingly, the second peak for the ponderosa pine areas is more pronounced and occurs one spectral band (approximately 10nm) earlier than in the plots for the mixed conifer and red fir areas. Also, in the region 1.52-1.57 um, the mixed conifer and red fir plots are considerably flatter than the ponderosa pine plots.

In the spectral plots for Grating Position 1 (Figure 15), again the most obvious feature is the general difference in the magnitude of reflectance between some of the forest areas. However, two sites in this graph, one mixed conifer and one red fir, have almost identical response curves. The ponderosa pine area has markedly higher reflectance than the other areas. The variation in shapes of the

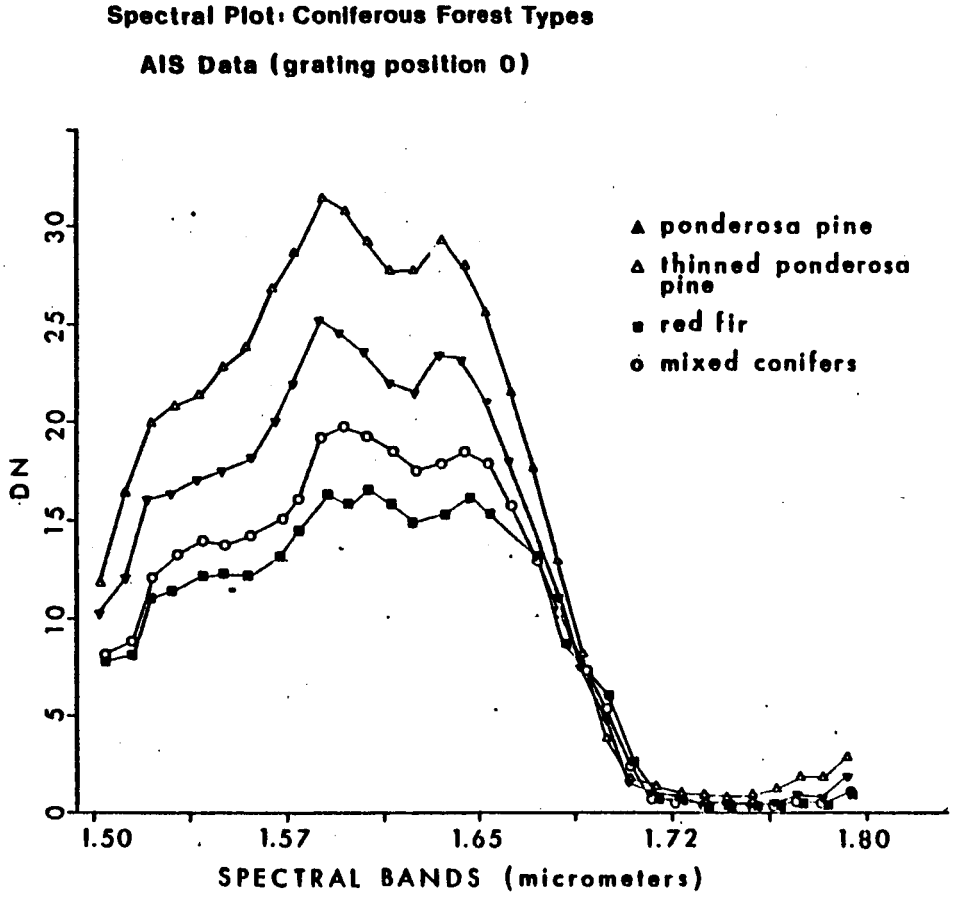

Figure 14. Spectral response curves in the 1.5-1.8 um region for four forest types.

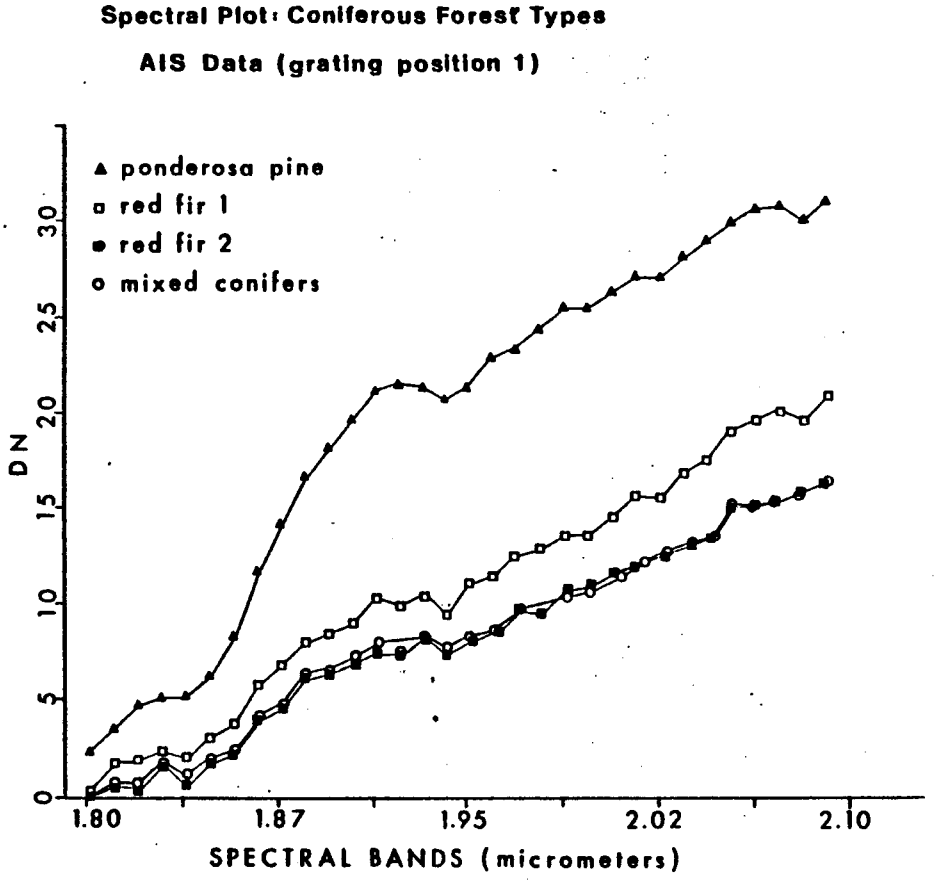

Figure 15. Spectral response curves in the 1.8-2.1 um region for four forest types.

plots is even more subtle than in Grating Position 0. The small drop in reflectance at about 2.09 um in one of the red fir sites and in the ponderosa pine site might be important, as could be the sudden jump in reflectance at 2.05 um for the red fir and mixed conifer sites.

4. PHASE II

The second part of this study, Phase II, consisted of computer-aided analysis of the AIS data. This second phase was broken down into three steps: (1) principal components analysis, (2) comparison of old calibrated with new

calibrated data, and (3) analysis of between-band ratios.

4.1. PRINCIPAL COMPONENTS

In his analysis of AIS data from the Pico Anticline, Rock [3] showed that principal components images of AIS data had considerable potential to differentiate among community types. Accordingly, we performed principal components transforms (actually, Karhunen-Love transforms) on AIS data for a section of the Grass Lake transect including the Lake and its surrounding shore. We limited our analysis to this area because large portions of the remaining images were obscured by cloud cover. Of the three spectral transects, only two were sufficiently cloud-free in the vicinity of the Lake to use in the analysis. Thus, the discussion below is restricted to grating positions 0 and 2. We also had to reduce the number of channels input to principal components transform because the VICAR program EIGEN is limited to ten input channels. Accordingly, we chose every third channel from the center of each spectral range.

Tables 1 and 2 present the loadings of the channels on each of the first four components for grating positions 0 and 2. The loadings for grating position 0 present a pattern expected for data that are repetitions of a more or less smooth, undulating spectral curve. All channels load positively on the first component, showing a tendency for overall brightness in all channels to be similar. The second principal component reflects the tendency of the

Table 1. Principal Component Analysis, Grating Position 0

Channel	Principal Component			
	1	2	3	4
	Loadings			
3	.1562	-.2125	.1926	.0321
6	.2304	-.3287	.3337	.1736
9	.2770	-.3290	.4479	.1221
12	.3723	-.2536	.2297	-.4757
15	.4056	-.1002	-.4295	-.4547
18	.4209	-.1224	-.5367	.1448
21	.3732	.0394	-.1608	.5780
24	.2922	.3308	.1117	.3290
27	.2637	.5046	.2035	-.1667
30	.2670	.5326	.2144	-.1725
	Eigenvalues			
	1717	453	40	31

spectral measurements to increase or decrease as wavelength increases. The third component detects an inflection in the center of the spectral curve, and the fourth component picks up a third-order trend. For grating position 2, the result is similar. The first component represents overall brightness, and the others detect various degrees of curvilinearity with the spectrum.

Figures 16A and 16B present the final images for grating positions 0 and 2 respectively. The image strips show

Table 2. Principal Component Analysis, Grating Position 2

Channel	Principal Component			
	1	2	3	4
	Loadings			
3	.2751	-.3612	-.1356	.3616
6	.2580	-.3608	.0199	.4406
9	.3262	-.4088	-.1059	-.0897
12	.3473	-.3071	-.3228	-.4510
15	.3563	.2794	-.3049	-.3498
18	.3445	.5135	-.2070	.0544
21	.3447	.3397	-.0419	.5120
24	.3164	.1186	.0896	-.0004
27	.2922	-.0543	.5379	-.2674
30	.2862	.0610	.6563	-.0684
	Eigenvalues			
	737	73	64	37

ORIGINAL PAGE
COLOR PHOTOGRAPH

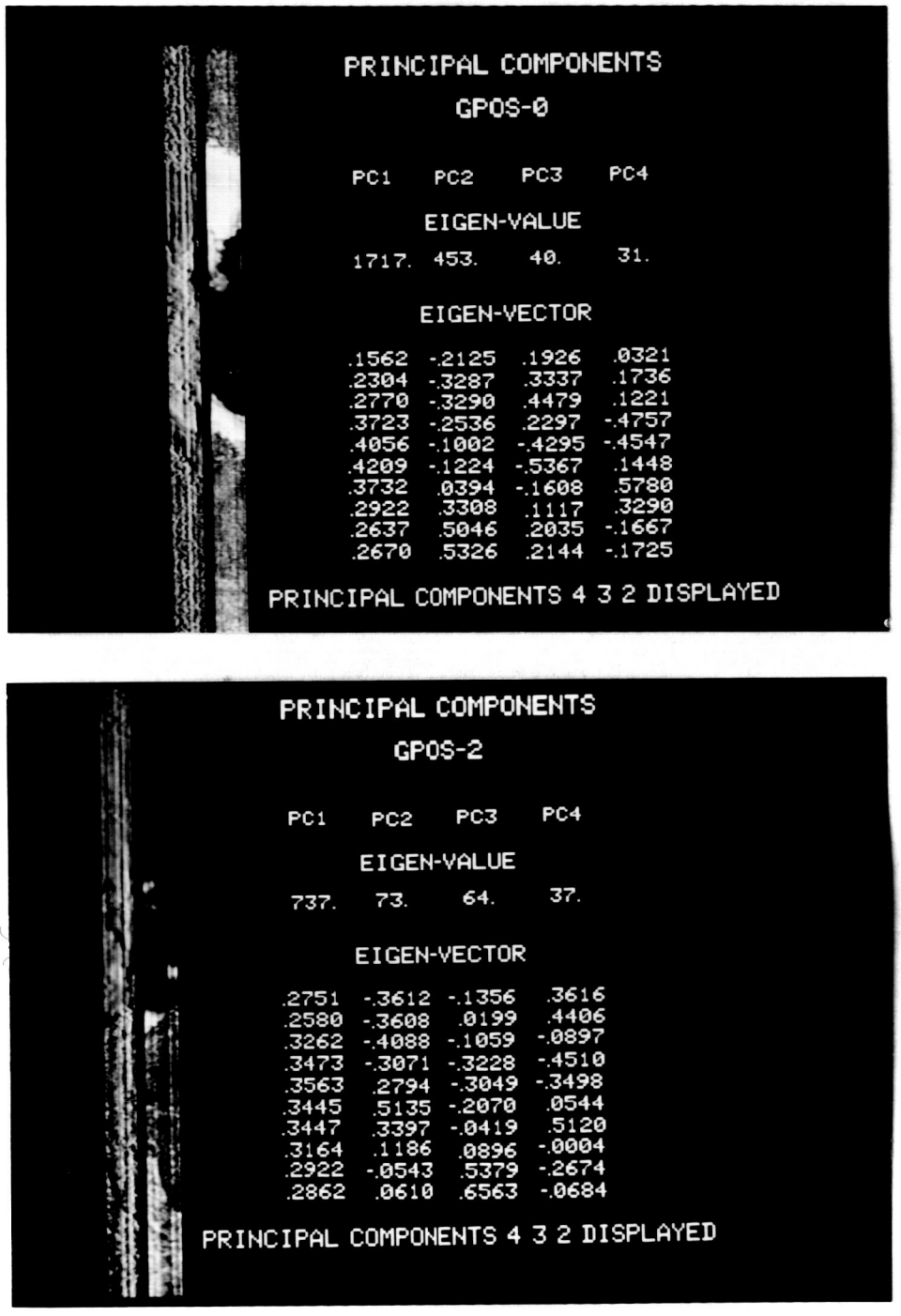

Figure 16. Principal components analysis for GPOS 0 (A, upper) and GPOS 2 (B, lower) images.

transects across Grass Lake displayed as color images of principal components 4, 3 and 2 assigned the colors red, green and blue, respectively. Also displayed is a single-band image in back and white to serve as a location finder. In both transects, the principal components strongly enhance the striping found in the original images. In Figure 16A, the water of the lake is obviously differentiated from the surrounding vegetation and from the small cloud directly above the lake. Within the lake, some spots of magenta may be picking up shallow areas with aquatic plants close to the surface. The light area of wet marsh just below the lake is clearly separated from cloud. (Note that the two transects are slightly offset in this display.) However, the remaining vegetation does not show much differentiation that is above the level of variation in individual detectors. In Figure 16B, magenta tones seem to identify light areas in the normally-displayed transect. Some of these are within the lake, while others are on the adjacent shores. The pattern does not seem to reflect the zonation present in the area at the time of the ground truth.

4.2. RECALIBRATED DATA

At the about the time that the principal components analysis was completed, we received newly-calibrated data from JPL. Although the data were of improved quality, we were unfortunately unable to repeat the principal components analysis; however, the new data were used in studies of band

ratios as described below.

Figure 17 compares the old and newly-recalibrated data for two strips containing Grass Lake taken from the image for grating position 0. This area is also shown in the principal components figure (Fig. 16A). The recalibrated data are significantly clearer, and reveal detail absent in the earlier data. The striping is still prominent, however. Figures 18A and B are similarly taken from the second grating position, but are enlarged by 2x for greater clarity. The enhanced detail and contrast of the recalibrated data are evident. For example, there is a road crossing the bottom of the strip in Figure 18B that cannot be discerned in the old data but is quite obvious in the recalibrated data.

4.3. RATIOS

One means of comparing spectral signatures is through band ratios. Selected ratios can enhance the spectral separation of objects, especially in the presence of overall variations in brightness that can confound identification.

In the spectral plots for Grating Position 0 of the Grass Lake test site, a "dip" was noticed in the curves for red fir and dense ponderosa between bands 14 (nominally 1.34 um), 15 (1.35 um), and 16 (1.36 um). However, the dips were of unequal magnitude, thus suggesting a mechanism for separating these two conifer species. Accordingly, we prepared ratio images of bands 15 to 16 and 15 to 14 for analysis. In order to carry this out more effectively, we

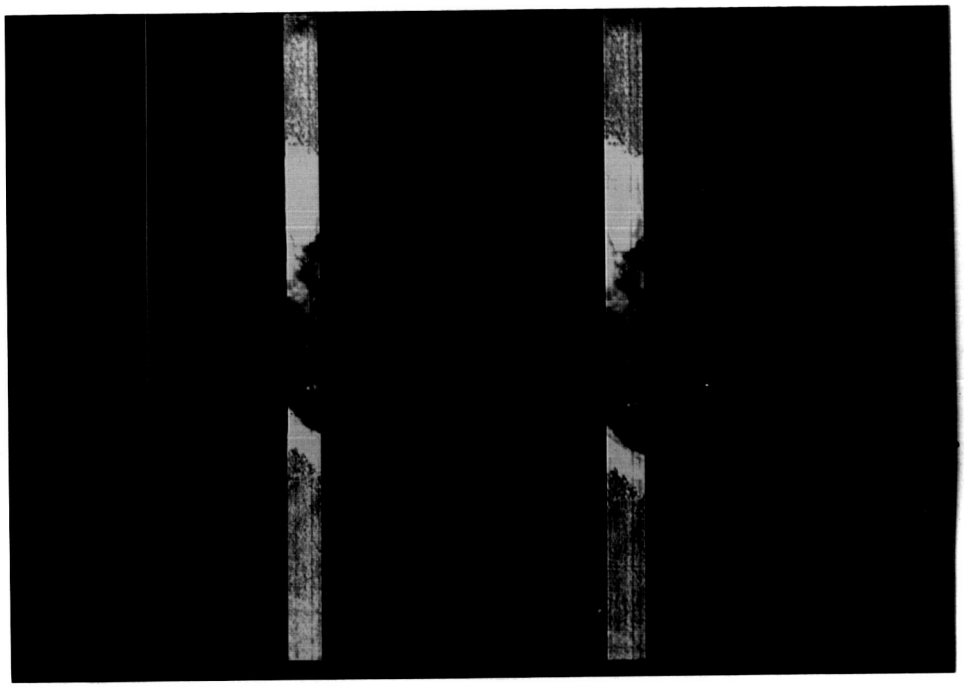

Figure 17. Old (left) and newly recalibrated (right) data for the GPOS 0 transect.

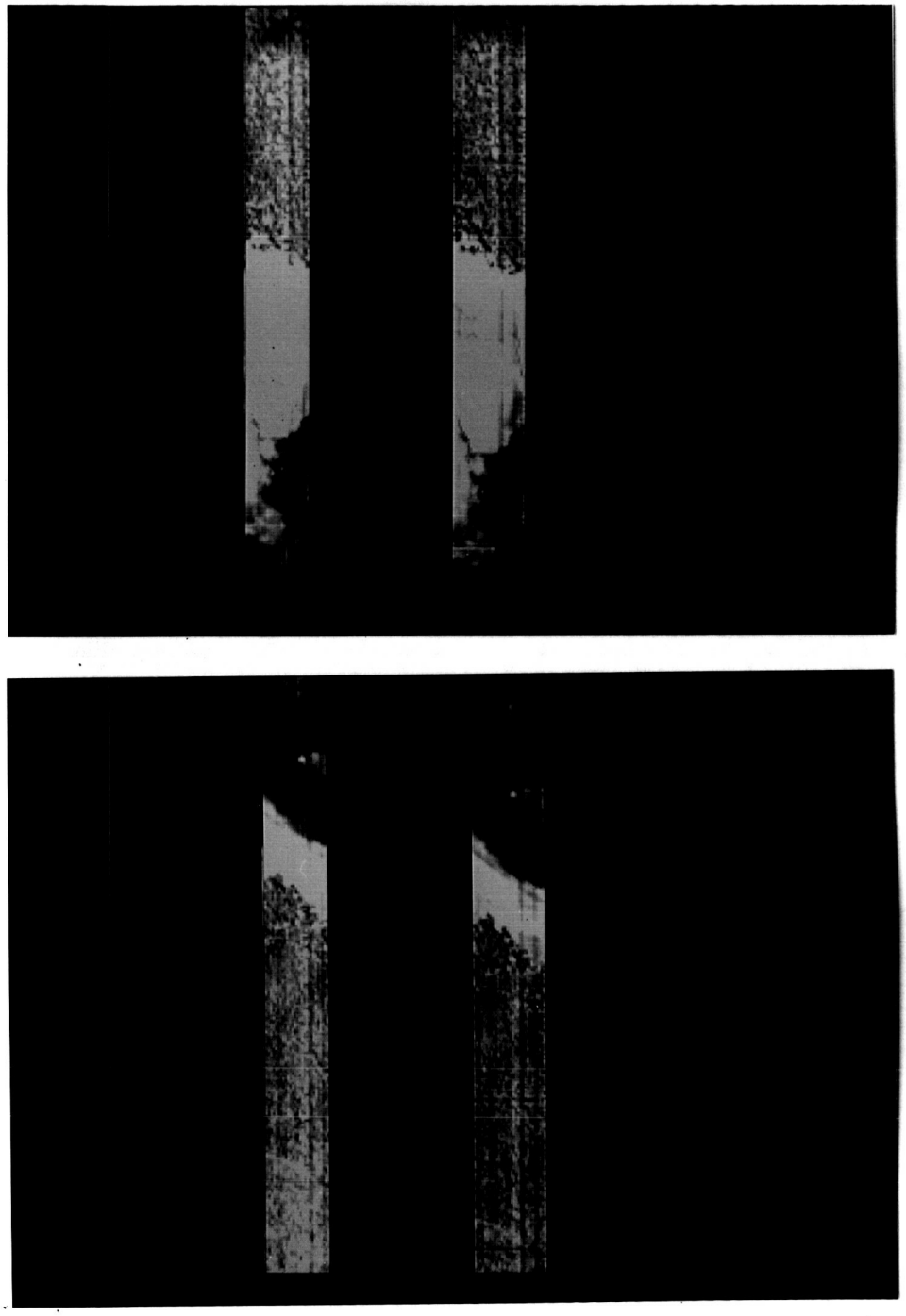

Figure 18. Close-up of Figure 17 at north (upper) and south (lower) edges of Grass Lake.

removed alternate lines from each single-band image, divided it into 512-line segments, and then stacked all the segments together to fit into a single 512-by-512 image. The resulting image of band 14 is displayed in Figure 19.

Figures 20 and 21 present the 15/16 and 15/14 ratios respectively for the Grass Lake transect. Unfortunately, the ratios reveal little information. The images are dominated by banding, blackouts, and a rhythmic rising and falling in overall brightness. There are no patterns that seem to make sense in light of the ground truth. Only the third strip from the right in the 15/14 image appears to have some information content; this half of the ratio image is presented along with the original band 15 values in Figure 22. Since there is nothing remarkable in the original band image of this segment, it appears likely that the pattern is an artifact caused by having one of the band 15 or 14 images offset with respect to the other by a line or two before calculating the ratio.

The 15/14 ratio was also calculated for the data collected from the Dock Well test site (Figure 23). As in the case of the Grass Lake transect, there appeared to be little information of value in the ratio.

4.4. BAND-RATIO STATISTICS

In a last attempt to examine the utility of the band ratios, we selected six sites representing six divergent vegetation types: red fir, lodgepole pine, brush, sparse

ORIGINAL PAGE
COLOR PHOTOGRAPH

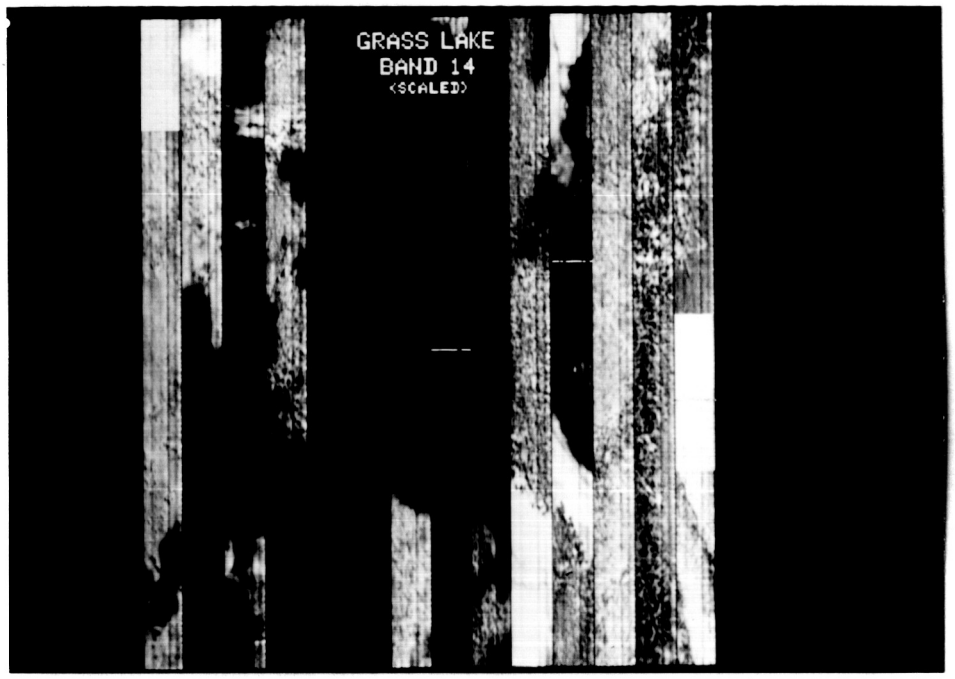

Figure 19. Band 14 of the GPOS 0 Grass Lake transect.

Figure 20. Image displaying ratio of bands 15 to 16 in the GPOS 1 image of the Grass Lake transect.

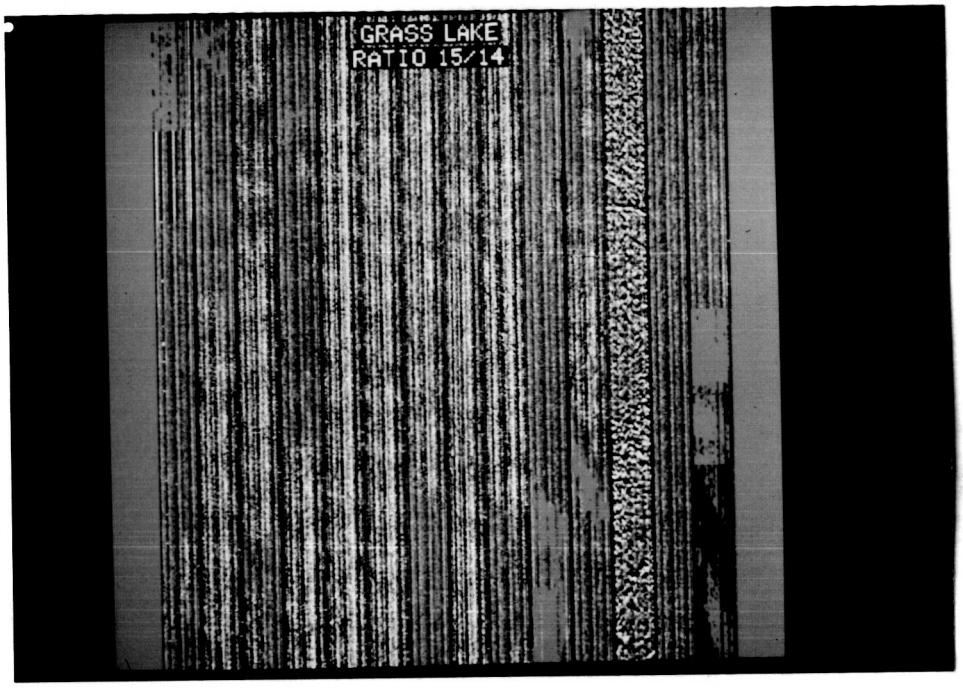

Figure 21. Image displaying ratio of bands 15 to 14 in the GPOS 1 image of the Grass Lake Transect.

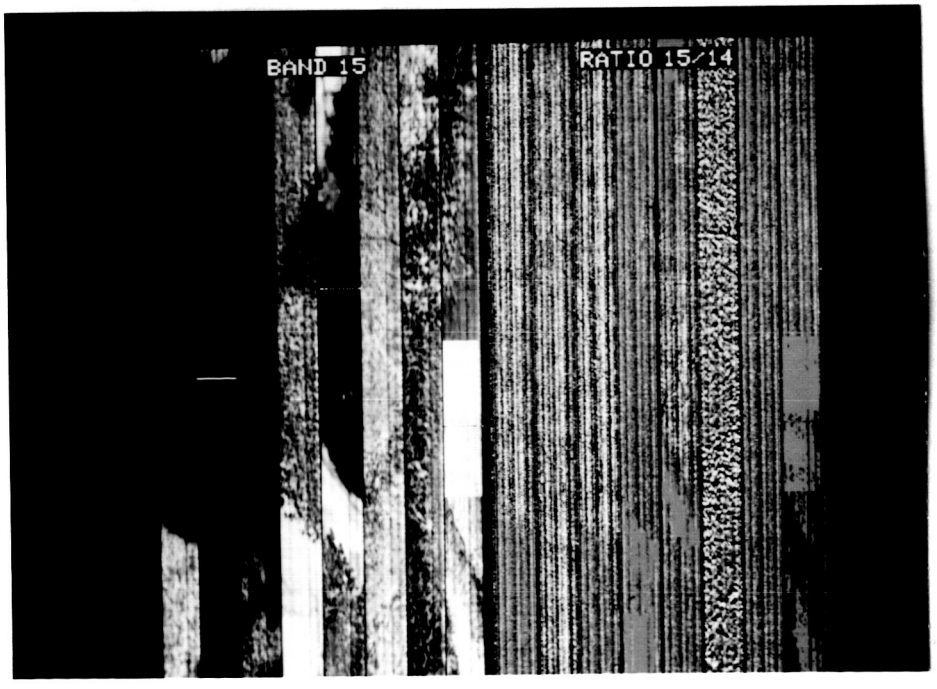

Figure 22. Comparison of band 15 and 15/14 ratio images.

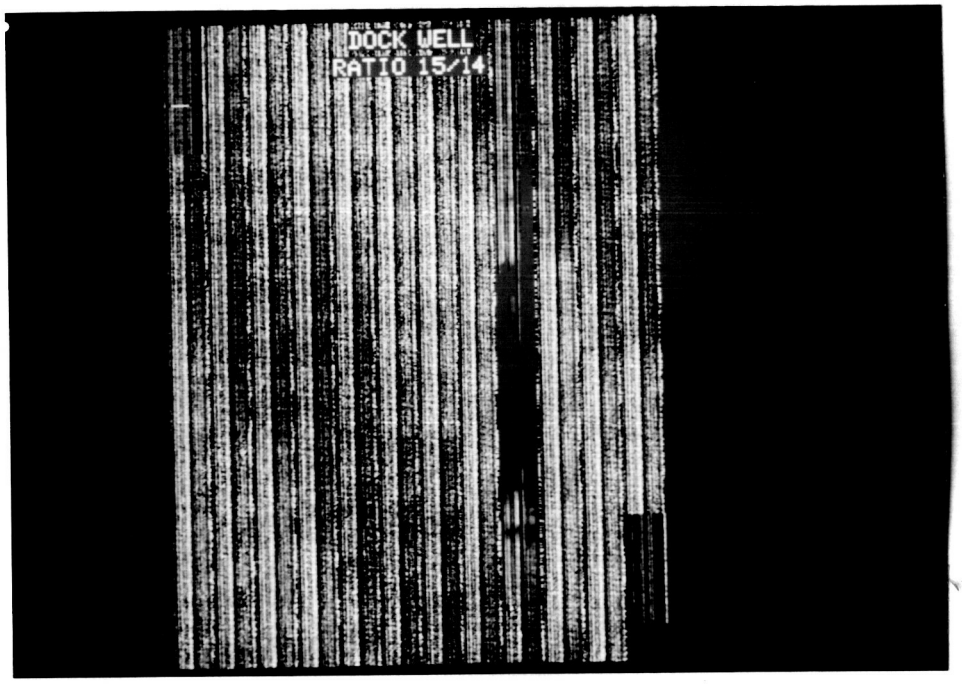

Figure 23. Ratio image of GPOS 1 bands 15 to 14 for the Dock Well transect.

ponderosa/Jeffrey pine, dense ponderosa/Jeffrey pine, and mixed conifer. Each site was delineated on the band-ratio imagery and training statistics for each were calculated -- these are shown in Table 3.

The table shows that the pixel-to-pixel variation within each vegetation type was very great, with coefficients of variation (ratio of standard deviation to mean) of around .5. The table also shows the standard error of the mean for each type. Since the means are based on large numbers of pixels, the standard errors are quite small. Figure 24 plots each type by ratio and includes error bars

Table 3. Statistics for Band Ratios.

Ratio	Statistic	Site Type: Red Fir	Lodge-pole	Brush	Sparse PoP	Dense PoP	Mixed Conif
15/14	Mean	127.3	142.9	133.0	123.1	128.0	128.4
	Std. Dev.	71.6	68.1	60.4	64.7	66.2	75.0
	Std. Err. of Mean	2.5	2.7	2.4	2.3	3.9	3.3
15/16	Mean	108.0	98.9	95.3	90.0	95.5	105.7
	Std. Dev.	60.0	48.9	35.8	48.5	41.9	58.9
	Std. Err. of Mean	2.1	1.9	1.4	1.7	2.4	2.6
	Sample No.	855	637	663	828	300	528

indicating the standard error of the mean for each ratio. In the figure, the 15/14 ratio separates the three open-canopy types from the three closed-canopy types, and the 15/16 ratio separates the red fir and mixed conifer types from the remaining four. On the two axes, all but the red

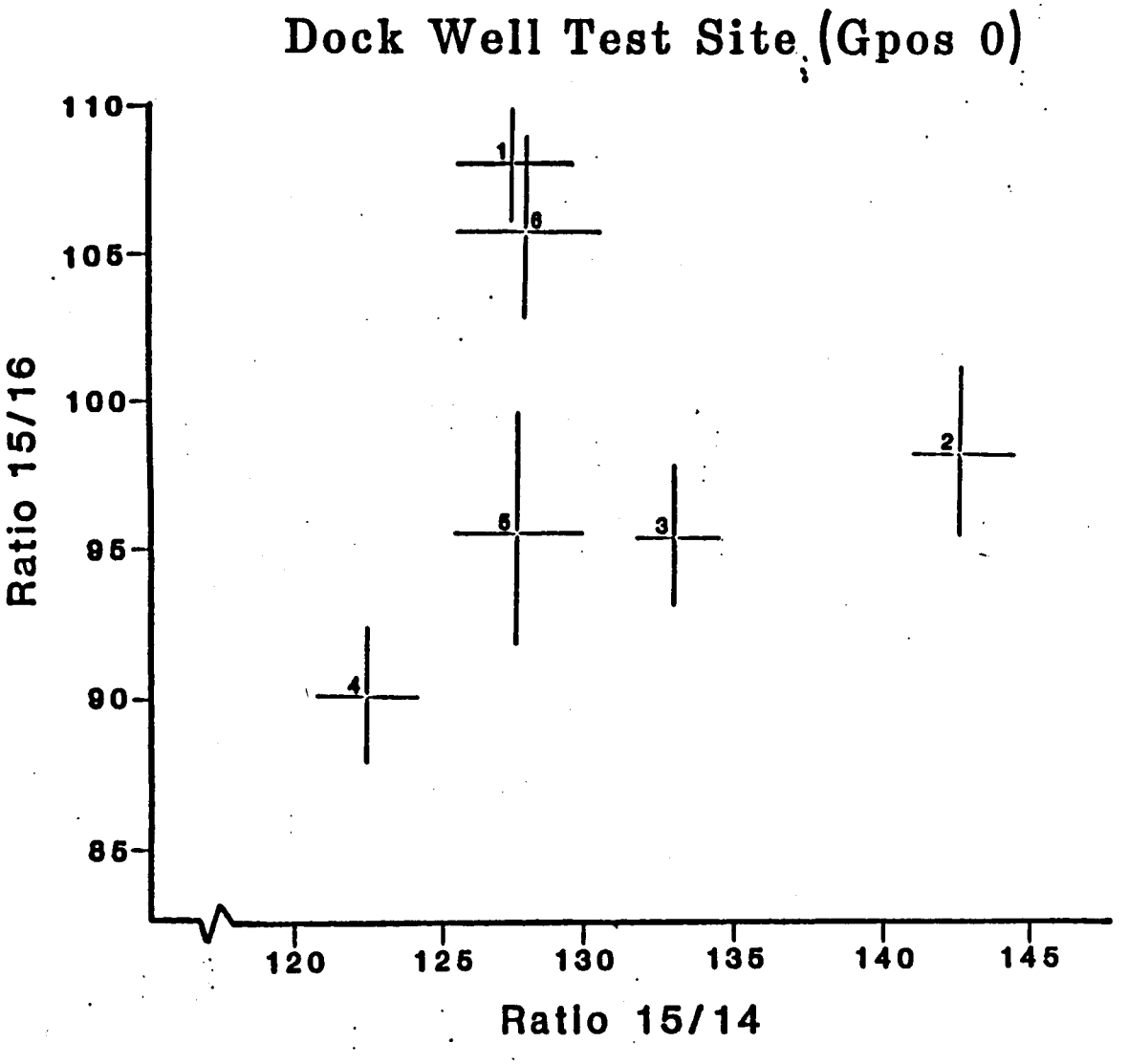

Figure 24. Plots of band ratios for six different vegetation types.

fir and mixed conifer types are easily differentiated.

Although the types are largely separable in the figure, it is only by virtue of the large sample size that each is distinguishable. The results are thus best interpreted as weak tendencies toward spectral differentiation that are manifest with large samples but are far too weak for pixel-by-pixel classification.

5. CONCLUSION

High spectral resolution remote sensing is one of the most exciting developments in space science in the last decade. The ability to determine the spectral reflectance of individual pixels in hundreds of contiguous narrow spectral bands will provide great benefits for the improved understanding of global phenomena and better utilization of earth resources. However, the link between high resolution remote sensing and ground information that will be required for such benefits is still being explored. Although much is known about the spectral responses of individual minerals that are of economic interest to the geologist, little is known about the potential to differentiate plants and community types through such high resolution spectra. Our studies present a first attempt.

Although our analysis of the AIS imagery did not suggest that tree species and vegetation types are easily differentiated by spectral response curves in the 1.2-2.1 um region, it is not possible to conclude that high spectral-

resolution remote sensing will not prove helpful in this regard. The data were gathered by a one-of-a-kind experimental instrument, and were not of the quality likely to be delivered by a second- or third-generation instrument. There were also further problems with clouds at the time of the second overpass, and accompanying problems with the timing of field reconnaissance work to support the observations.

However, a few truths do seem to emerge from our study. First, vegetation signatures in the near-infrared are all seem to be basically similar. Although there are significant differences in overall brightness in spectral response, there do not seem to be well-developed spectral features that are analogous to absorption peaks in mineral spectra. Note that this observation probably only applies to the near-infrared -- in the visible, absorption features of chlorophylls and accessory pigments may well facilitate plant discrimination and identification.

Another conclusion is that effective methods for processing high spectral-resolution vegetation-reflectance data have yet to be developed. The binary classifier we tested at JPL, which is well suited to identifying characteristic features of mineral spectra, performs very poorly on vegetation spectra because of their similar shapes. The principal components analysis we carried out yielded equivocal results. The spectral plots demonstrate that overall

brightness helps separate vegetation types, but this effect, manifest in the first principal component, reflects general vegetation form and coverage only generally, and is not likely to be responsive to unique structures or species compositions that help separate plant communities. On the other hand, color composites of the second, third and fourth components, which respond to the overall shape of the spectral curves, do not show much information that can be related to phenomena on the ground. Perhaps future techniques will be more sensitive and help reveal spectral structure that did not emerge in our study.

6. BIBLIOGRAPHY

[1] Jet Propulsion Laboratory, 1984. Airborne Imaging Spectrometer: Science Investigator's Guide to AIS data, February 20, 1894.

[2] Holloway, J. L., 1958. Smoothing and filtering of time series and space fields: Advances in Geophysics, vol. 4, pp. 351-389.

[3] Rock, Barrett N., Citation for Pico Anticline needed.